NIH Public Access
Author Manuscript
FEBS Lett. Author manuscript; available in PMC 2015 April 17.

Published in final edited form as:
FEBS Lett. 2014 April 17; 588(8): 1458–1464. doi:10.1016/j.febslet.2014.01.010.

Atrial fibrillation-associated Connexin40 mutants make hemichannels and synergistically form gap junction channels with novel properties

Dakshesh Patel[1], **Joanna Gemel**[2], **Qin Xu**[1], **Adria R Simon**[2,†], **Xianming Lin**[1,*], **Arvydas Matiukas**[1], **Eric C Beyer**[2], and **Richard D Veenstra**[1,3]

[1]Department of Pharmacology, SUNY Upstate Medical University, Syracuse, NY 13210

[2]Department of Pediatrics, University of Chicago, Chicago, IL 60637

[3]Cell and Developmental Biology, SUNY Upstate Medical University, Syracuse, NY 13210

Abstract

Mutations of Cx40 (*GJA5*) have been identified in people with lone chronic atrial fibrillation including G38D and M163V which were found in the same patient. We used dual whole cell patch clamp procedures to examine the transjunctional voltage (V_j) gating and channel conductance properties of these two rare mutants. Each mutant exhibited slight alterations of V_j gating properties and increased the gap junction channel conductance (γ_j) by 20–30 pS. While co-expression of the two mutations had similar effects on V_j gating, it synergistically increased γ_j by 50%. Unlike WTCx40 or M163V, G38D induced activity of a dominant 271 pS hemichannel.

Keywords

atrial fibrillation; gap junctions; hemichannels; connexin40; channel conductance

INTRODUCTION

Atrial fibrillation (AF) is the most common form of cardiac arrhythmia in the human population. AF is characterized by a rapid and irregular electrical activation and the loss of atrial muscle contractility. Conduction of the cardiac action potential depends primarily on activation of the cardiac sodium current and the intercellular electrical communication mediated by gap junction channels. Gap junctions are specialized intercellular junctions formed by members of the connexin family of proteins which assemble into hexameric

© 2014 Federation of European Biochemical Societies. Published by Elsevier B.V. All rights reserved.

Corresponding Author: Richard D. Veenstra, Ph.D., Department of Pharmacology, SUNY Upstate Medical University, 750 East Adams Street, Syracuse, NY 13210, Ph: 315-464-5145, Fax: 315-464-8014, veenstrr@upstate.edu.
*Dr. Lin's present address is the Leon H. Charney Division of Cardiology, New York University School of Medicine, New York, NY 10016
†Ms. Simon's current address is New York University School of Medicine, New York, NY 10016

Publisher's Disclaimer: This is a PDF file of an unedited manuscript that has been accepted for publication. As a service to our customers we are providing this early version of the manuscript. The manuscript will undergo copyediting, typesetting, and review of the resulting proof before it is published in its final citable form. Please note that during the production process errors may be discovered which could affect the content, and all legal disclaimers that apply to the journal pertain.

NIH-PA Author Manuscript
NIH-PA Author Manuscript
NIH-PA Author Manuscript

NIH-PA Author Manuscript

NIH-PA Author Manuscript

NIH-PA Author Manuscript

hemichannels that dock to form intercellular channels for the passage of ions, second messengers, and small soluble molecules [1]. Twenty different connexin gene products are expressed in various human tissues. Mutations of different family members have been identified as genetic causes of human diseases including deafness, neuropathy, cataracts, skin disorders, craniofacial malformations, and cardiac arrhythmias. Most commonly, the disease-linked connexin mutations result in loss-of–function due to protein truncation, impaired trafficking/assembly, or disruption of channel activity. Rarely, “gain-of-function” connexin mutants have been identified that lead to aberrant enhancement of hemichannel currents [2,3].

Two connexins, connexin43 (Cx43) and connexin40 (Cx40), are abundantly expressed in the working myocardium of the atrium and are critical to conduction within this tissue. Mutations of Cx43 (*GJA1*) have mostly been identified in patients with oculodentodigital dysplasia, a syndrome typically including skeletal abnormalities and only rarely associated with arrhythmias [4]. Recently, a Cx43 deletion mutant was associated with atrial fibrillation [5]. In contrast, several mutations of Cx40 (*GJA5*) have been specifically associated with enhanced atrial vulnerability and fibrillation [6,7]. In the first report of Cx40, one chronic AF patient expressed two non-allelic somatic mutations, G38D and M163V [6]. Each connexin monomer contains 4 transmembrane domains (M1-4) separated by two extracellular domains (E1 and E2) and a cytoplasmic loop(CL). G38D and M163V are located within M1 and M3, close to the extracellular and cytoplasmic surfaces of the membrane, respectively (Fig. 1A). Both Cx40 mutants were functional when studied in an *in vitro* expression system, and a sparse, mosaic distribution of Cx40 gap junctions was observed in right atrial appendage biopsies from the patient [6]. The authors postulated that M163V was a benign polymorphism and that the G38D mutation caused subcellular retention of the Cx40 protein with impaired formation of gap junction plaques, but the gap junctions that did form functioned normally [6].

In the current study, we expressed the rare human G38D and M163V Cx40 mutants alone and together to examine their formation of intercellular channels and hemichannels and the electrical properties of those connexin channels. We have identified some modest alterations of individual channel properties, but our findings also suggest that cooperative interactions occur between two distinct mutant connexin subunits resulting in significantly different gap junction channel properties than predicted from the behavior of either mutant alone.

MATERIALS AND METHODS

Connexin-expressing cells

Human Cx40 DNA was subcloned into pSFFV-neo[8], pTracer-CMV2(Life Technologies), pEGFP-N1 (Clontech) or 6B-mCherry (plasmid 30125, Addgene) eukaryotic expression plasmids. Mutants of human Cx40 containing substitutions G38D and M163V were generated with the QuickChange Site-Directed Mutagenesis Kit (Agilent Technologies UK, Ltd.). HeLa and N2a cells were cultured and transiently transfected using Lipofectamine 2000 (Life Technologies) as previously described [8,9]. For immunofluorescence and immunoblot analysis of connexin expression, HeLa cells were transfected with constructs in pSFFV-neo. For the electrophysiological experiments, N2a cells were transiently transfected

NIH-PA Author Manuscript

NIH-PA Author Manuscript

NIH-PA Author Manuscript

with connexin DNAs in pTracer-CMV2, pEGFP-N1 or 6B-mCherry to facilitate identification of transfected cells based on green (EGFP) or red (mCherry) fluorescence or both (co-expression).

Immunodetection of connexins

Cx40 was detected using rabbit polyclonal antibodies (Invitrogen). For double-labeling experiments, cells were incubated simultaneously with both mouse anti-mCherry monoclonal and rabbit anti-GFP antibodies (Abcam). Immunoblots were performed as described earlier [10] using cell homogenates prepared 48 h after transfection with connexin DNA as described by Gong *et al*. [11]. For immunofluorescence microscopy, cultured cells were fixed in methanol/acetone (1:1), stained as previously described [8], and imaged using a Zeiss Axioplan 2 microscope or Leica TCS SP2 laser-scanning confocal microscope.

Gap junction conductance measurements

Dual whole cell patch clamp experiments were performed using conventional 140 mM NaCl or KCl bath saline or patch electrode solutions and junctional conductance-voltage curves were corrected for series resistance errors as previously published [12]. Steady-state $g_j - V_j$ relationships were normalized by dividing g_j by the linear slope g_j (g_{max}) value for each experiment ($G_j = g_j/g_{j,max}$) and fitting each voltage polarity of the G_j-V_j curve with the typical two state Boltzmann equation as previously described [12,13]. Fitted curves were calculated using Clampfit software (Molecular Devices) using the sum of squared errors minimization procedure, and graphs were prepared using Origin7.5. Statistical analysis of gap junction channel slope conductances was performed using the *F-test* Comparison of Two Datasets function in Origin7.5.

Cx40 gap junction channel current amplitudes and G38D hemichannel current amplitudes were measured from Gaussian fits of all points current amplitude histograms using previously described procedures [14]. V_j was stepped from 0 to ±50 mV in 10 mV increments in 30 sec intervals with a 30 sec rest period between pulses. Data were amplified to 50 mV/pA, low pass filtered at 200 Hz, acquired at 2 kHz using pClamp8.2 or 10.1, and converted to all points histograms (0.1 pA bin width) using Origin 7.5 or 8.6 for multi-peak Gaussian fits of the resultant current amplitude histogram. Single channel current amplitudes were measured as the mean difference between adjacent Gaussian peaks. The mean currents were determined for all statistically measured Gaussian peaks visible in the current amplitude histogram. Infrequent or small amplitude events that could not be resolved by Gaussian fits of the amplitude histogram were not measured.

Hemichannel current measurements

To record whole cell hemichannel currents, the same patch clamp procedures were performed on single N2a cells bathed in a zero $CaCl_2$, 11 mM glucose saline solution. An 8 sec −80 to +80 membrane potential (V_m, 50 ms per 1 mVstep staircase) ramp protocol was applied to individual N2a cells based on the methods of Sanchez et al. [15]. To activate any potential hemichannels, N2a cells were stepped to peak voltages of +20 or +30 mV and hyperpolarized to −40 mV or various potentials from 0 to −90 mV for 10 sec per interval. Whole cell currents were low pass filtered at 200 Hz, digitized at 2 kHz, and all points

NIH-PA Author Manuscript

NIH-PA Author Manuscript

NIH-PA Author Manuscript

current histograms were generated using Origin and fitted with Gaussian peaks to measure the peak-to-peak current amplitudes.

RESULTS

The production of wild type (WT) Cx40, G38D, or M163V protein and their assembly into gap junctions were studied in stably transfected HeLa cells. Immunoblots showed that each of the constructs produced immunoreactive Cx40 protein consisting of bands with similar electrophoretic mobilities (Fig. 1B). Immunofluorescence microscopy showed that WTCx40 and both mutants localized similarly within the transfected cells: within the cytoplasm (in a distribution consistent with the biosynthetic pathway) and in punctae at plasma membrane appositions (consistent with gap junctions) (Fig. 1C).

Dual whole-cell patch-clamp recordings from pairs of transiently transfected N2a cells showed that high levels of gap junctional conductance (g_j) were produced by WTCx40, G38D (89%, n=65), and M163V (83%, n=65) regardless of the absence or presence of an EGFP tag. V_j-dependent gating was examined in cell pairs with low g_j values (Table S1). Both mutants had shifted V_j gating profiles as illustrated by the normalized G_j-V_j curves obtained after application of ±120 mV, 200 ms/mV V_j ramps (Fig. 2A, Table 1). Similarly to our previous studies of rat Cx40 [15], human WTCx40 showed V_j-dependent gating with half-inactivation voltage ($V_{½}$), ±44 mV and gating charge valence (z) ≈3.8 electron equivalents (q) (Table 1). $V_{½}$ was reduced by ~10 mV for G38D and increased by 5 mV for M163V. Both Cx40 mutations reduced the gating charge valence by 1.0–1.5 q, indicating reduced V_j-sensitivity despite opposite shifts in the applied V_j gradient required to effect the gating transition from the open to the minimum junctional conductance ($G_{j,min}$) state of the gap junction.

Since the original patient with AF expressed G38D and M163V from separate alleles [6], we wanted to understand the properties conferred by co-expression of these two rare mutants. Cells were transiently transfected with G38D-EGFP and M163V-mCherry (which extensively co-localized at appositional membranes, Fig. 2B). Co-expressing N2a cell pairs contained gap junction channels that were phenotypically distinct from WTCx40 or either mutant when expressed alone. All G38D/M163V cell pairs were coupled (n=21), with 11 that were highly coupled and one that was so poorly coupled to allow resolution of single channel currents. The G_j-V_j curve determined from G38D+M163V co-expressing cells was shifted outward by 10 mV relative to WT (Fig. 2A). The gating charge valence (*z*) resembled that of G38D while the half-inactivation voltage ($V_{½;}$ ≈±55 mV) was shifted further outward than even the most severely affected mutant (M163V) alone (Table 1).

Gap junction channel currents obtained from poorly coupled N2a-Cx40 cell pairs allowed identification and analysis of single channel events. WTCx40 had a unitary conductance (γ_j) of 149±2 pS (Fig. 3A, B), like rat Cx40 [14,16]. G38D produced a 20% larger channel with a γ_j of 178±2 pS(Fig. 3C, D). The γ_j of M163V channels was increased by 20 pS to 169 ± 2 pS (Fig. 3E, F). Thus, each fluorescent protein-tagged mutant had a γ_j that was significantly greater than that of WT ($p<0.05$). Co-expression of G38D and M163V increased the main state γ_j by ≈50% to 218±5 pS (n=2, much more than either mutant alone) (Fig. 3 G,H).

NIH-PA Author Manuscript

NIH-PA Author Manuscript

NIH-PA Author Manuscript

We also examined the ability of these mutations to produce functional hemichannels in the absence of external calcium. Fig. 4A illustrates the whole cell current response of untransfected N2a, stable N2a-Cx40, and transiently transfected G38D, M163V, and G38D +M163V N2a cells to a 160 mV, 8 sec (50 ms/mV) staircase ramp of membrane potential (V_m). Despite similar whole cell current values for all cells, only G38D and G38D+M163V cells exhibited hemichannel open-closed events. The −80 to +80 mV whole cell current recordings for all experimental groups and their averages are displayed in Supplemental Figures S1–S5. Since the G38D mutation produced dominant hemichannel currents, this mutant Cx40 hemichannel activity was studied using V_m step protocols from −40 mV to activating potentials of +20 or +30 mV for 10 sec, returning to −40 mV or various hyperpolarized potentials. One such +20 to −40 mV pulse protocol sequence is illustrated in Fig. 4B where approximately three G38D hemichannels were observed to open with depolarization and close again with hyperpolarization, inclusive of a subconductance state. The G38D hemichannel current amplitudes were measured in three experiments during V_m pulses to +20 or +30 mV and subsequent repolarization to negative V_m values from −20 to −80 mV. The resultant current-voltage yielded a slope conductance of 271±10 pS. The hemichannel conductance (γ_{hc}) was only 50% greater than the γ_j for G38D, but nearly twice the γ_j value of the WTCx40 channel. The G38D hemichannel activity decreased with the addition of 2 mM $CaCl_2$ in one long-lasting experiment (Fig. S6).

DISCUSSION

Our data obtained from homomeric expression of the G38D and M163V Cx40 mutations in HeLa and N2a cells confirm that both AF mutations form gap junction plaques and functional intercellular channels. Gollob *et al*. suggested that the M163V mutation might be benign, since it formed gap junction plaques and induced normal levels of electrical coupling [6]. In contrast they found that G38D-expressing cells had a three-fold reduced level of electrical coupling and were more rounded with increased cytoplasmic Cx40 content, suggesting increased mutant protein retention [6]. Our results with M163V were similar, but we found more appropriate trafficking and level of function with G38D. Perhaps the expression approaches were more permissive in our experiments.

The disease causing effects of connexin mutations are commonly ascribed to “loss-of-function” due to impaired protein folding/trafficking/assembly or disruption of gap junction channel function. The absence of such abnormalities suggests dysregulation of hemichannel or gap junction channel properties as an alternative consequence of the G38D and M163V mutations. Our functional analysis of G38D and M163V expressed individually revealed that each mutation produced slight changes in $V_{½}$ (increased or decreased by ~10 mV). G38D decreased the gating charge by ~1.5q, consistent with the previously defined role of the E1 loop in V_j gating [17]. The greatest change observed with the individually expressed mutants was the 20% increase in γ_j for G38D. This increase might have resulted from G38D causing reduced selectivity of the modestly (6:1) cation-selective 150 pS Cx40 gap junction channel [14], but we could not test this hypothesis because mutant channel recordings were difficult to obtain. Regardless, it seems unlikely that any of the altered gap junction channel properties of the individual mutants are sufficient to explain the development of atrial arrhythmias.

NIH-PA Author Manuscript

NIH-PA Author Manuscript

NIH-PA Author Manuscript

When studied in single cells, G38D (but not WTCx40 or M163V) consistently produced hemichannel currents in the absence of external Ca^{2+}. Dominant mutations causing the gain of connexin hemichannel function have been implicated in the disease pathogenesis of the Keratitis-Icthyosis-Deafness syndrome and cataracts that likely result from compromised cellular functions or death due to the "leaky" hemichannel currents [2,3,18]. Some of these mutations (Cx26G45E and Cx46G46V) alter amino acids near the M1/E1 interface, a region containing pore-lining residues that are critical for hemichannel gating [19]. Opening of G38D hemichannels would be expected to lead to cytotoxicity and might contribute to altered atrial conduction (especially if a somatic mutation was not uniformly expressed). We detected G38D hemichannels with a conductance (γ_{hc}) of only 271 pS, not the γ_{hc} of ~360 pS that might have been expected based on the γ_j of 178 pS G38D gap junctions. However, the estimated γ_{hc}/γ_j ratio of 2 is based on the assumption that the pore resistance is limited primarily by its length and not the access resistances encountered at both mouths of the pore. In actuality, the single channel conductance equals the arithmetic mean of the limiting ionic conductances only when $\frac{\overline{U}_{in}+\overline{V}_{out}}{\overline{U}_{out}+\overline{V}_{in}}=1$ where $\bar{U}$ and $\bar{V}$ are the limiting cation and anion conductances, respectively, of each side of the charged membrane channel pore, e.g. a symmetrical channel [20].

The greatest functional changes to the intercellular channels occurred when both mutations were co-expressed; matching the condition found in the lone AF patient by Gollob *et al*. [6]. Co-expression of these non-allelic Cx40 somatic mutations was not attempted in the original study. The G38D+M163V channels had a reduced gating charge (like G38D), an outward shift of $V_{½}$ (even further than that of M163V), and a 50% increase of the slope γ_j to 218 pS (greater than either individual mutant). These results are consistent with an additive effect of the two mutations on γ_j and a synergistic effect on the V_j gating properties in the channels containing both mutants. This is the first report of two unique connexin mutations occurring on separate subunits combining to produce functional changes in the resultant gap junction channel that exceed the effects observed with channels formed of either mutation alone. The V_j-gating effects might not contribute to atrial arrhythmias, since V_j-dependent gating does not occur unless g_j is low enough to produce millisecond delays in activation between adjacent cardiomyocytes [10,21]. However, the increased γ_j would affect the intercellular exchange of ions and second messenger molecules associated with an electrochemical gradient or a transient (<200 μs) V_j gradient as occurs during action potential propagation.

The effects of these mutations may be elucidated considering connexin polypeptide topology and gap junction channel structure. The G38D and M163V mutations reside on opposite sides of the membrane in adjacent transmembrane domains, with G38D located near the M1/E1 interface and M163V near the CL/M3 border. The G38D mutation would increase the negative electrostatic charge within the extracellular vestibule of a Cx40 gap junction channel (extracellular opening of an unpaired Cx40 hemichannel). This increased electro-negativity could account for the reduced half-inactivation voltage and gating charge and increased γ_j of G38D. The M163V mutation should increase the hydrophobicity near the M3/CL interface; this might increase $V_{½}$, assuming that translocation of the CL/M3 interface into a more hydrophilic environment is required for V_j gating. The increase in γ_j

NIH-PA Author Manuscript

NIH-PA Author Manuscript

NIH-PA Author Manuscript

associated with M163V suggests that it is near or influences part of the CL that contributes to the cytoplasmic vestibule of the channel. In the heteromeric channel, these opposite-sided membrane pore mutations appear to have additive effects on channel conductance, while the hydrophobic effects (in M163V) apparently dominate the $V_{½}$ gating alterations, and the charge altering mutation (in G38D) dominates the gating charge effects.

In summary, we have made a novel observation of synergistic functional changes in cells co-expressing two non-allelic connexins mutations that may explain why two mutants cause disease together. The interactions of G38D and M163V suggest structural interactions between the TM1/E1 and TM3/CL regions that influence the gating and channel conductance properties of gap junction channels. Moreover, G38D may also contribute to cell toxicity and arrhythmias by forming opening hemichannels.

Supplementary Material

Refer to Web version on PubMed Central for supplementary material.

Acknowledgments

The technical assistance of Laura Andrews and Li Gao is gratefully acknowledged. We also thank Dr. Scott Gradia (University of California, Berkeley) for making the mCherry-6B plasmid available through Addgene. This work was supported by NIH grants HL-059199 (ECB and RDV) and HL-042220 (RDV).

Abbreviations

Cx	Connexin
WT	Wild type
V_j	transjunctional voltage
I_j	Junctional current
γ_j	gap junction channel conductance
g_j	junctional conductance
G_j	Normalized junctional conductance
AF	Atrial fibrillation
V_m	membrane potential
M1-4	transmembrane domains
E1 and E2	extracellular domains
CL	cytoplasmic loop
EGFP	Enhanced green fluorescent protein
$V_{½}$	half-inactivation voltage
z	gating charge valence
q	electron equivalents

NIH-PA Author Manuscript

NIH-PA Author Manuscript

NIH-PA Author Manuscript

$G_{j\ min}$	minimum junctional conductance
γ_{hc}	hemichannel conductance

References

1. Harris AL. Connexin channel permeability to cytoplasmic molecules. Prog Biophys Mol Biol. 2007; 94:120–143. [PubMed: 17470375]
2. Lee JR, DeRosa AM, White TW. Connexin mutations causing skin disease and deafness increase hemichannel activity and cell death when expressed in *Xenopus* oocytes. J Invest Dermatol. 2009; 129:870–878. [PubMed: 18987669]
3. Minogue PJ, Tong JJ, Arora A, Russell-Eggitt I, Hunt DM, Moore AT, Ebihara L, Beyer EC, Berthoud VM. A mutant connexin50 with enhanced hemichannel function leads to cell death. Invest Ophthalmol Vis Sci. 2009; 50:5837–5845. [PubMed: 19684000]
4. Paznekas WA, Boyadjiev SA, Shapiro RE, Daniels O, Wollnik B, Keegan CE, Innis JW, Dinulos MB, Christian C, Hannibal MC, Jabs EW. Connexin 43 (*GJA1*) mutations cause the pleiotropic phenotype of oculodentodigital dysplasia. Am J Hum Genet. 2003; 72:408–418. [PubMed: 12457340]
5. Thibodeau IL, Xu J, Li Q, Liu G, Lam K, Veinot JP, Birnie DH, Jones DL, Krahn AD, Lemery R, Nicholson BJ, Gollob MH. Paradigm of genetic mosaicism and lone atrial fibrillation: physiological characterization of a connexin 43-deletion mutant identified from atrial tissue. Circulation. 2010; 122:236–244. [PubMed: 20606116]
6. Gollob DA, Jones DL, Krahn AD, Danis L, Gong XQ, Shao Q, Liu X, Veinot JP, Tang ASL, Stewart AFR, Tesson F, Klein GJ, Yee R, Skanes AC, Guiraudon GM, Ebihara L, Bai D. Somatic mutations in the connexin 40 gene (GJA5). N Engl J Med. 2006; 354:2677–2688. [PubMed: 16790700]
7. Yang Y-Q, Liu X, Zhang X-L, Wang X-H, Tan H-W, Shi H-F, Jiang WF, Fang WY. Novel connexin40 missense mutations in patients with familial atrial fibrillation. Europace. 2010; 12:1421–1427. [PubMed: 20650941]
8. Gemel J, Valiunas V, Brink PR, Beyer EC. Connexin43 and connexin26 form gap junctions, but not heteromeric channels in co-expressing cells. J Cell Sci. 2004; 117:2469–2480. [PubMed: 15128867]
9. Veenstra RD, Wang HZ, Westphale EM, Beyer EC. Multiple connexins confer distinct regulatory and conductance properties of gap junctions in developing heart. Circ Res. 1992; 71:1277–1283. [PubMed: 1382884]
10. Lin X, Gemel J, Glass A, Zemlin CW, Beyer EC, Veenstra RD. Connexin40 and connexin43 determine gating properties of atrial gap junction channels. J Mol Cell Cardiol. 2010; 48:238–245. [PubMed: 19486903]
11. Gong XQ, Shao Q, Lounsbury CS, Bai D, Laird DW. Functional characterization of a GJA1 frameshift mutation causing oculodentodigital dysplasia and palmoplantar keratoderma. J Biol Chem. 2006; 281:31801–31811. [PubMed: 16891658]
12. Veenstra RD. Voltage clamp limitations of dual whole cell recordings of gap junction current and voltage recordings. I Conductance measurements. Biophys J. 2001; 80:2231–2247. [PubMed: 11325726]
13. Spray DC, Harris AL, Bennett MVL. Equilibrium properties of a voltage-dependent junctional conductance. J Gen Physiol. 1981; 77:77–93. [PubMed: 6259274]
14. Lin X, Fenn E, Veenstra RD. An amino terminal lysine residue of rat connexin40 that is required for spermine block. J Physiol. 2006; 570:251–269. [PubMed: 16284078]
15. Sánchez HA, Orellana JA, Verselis VK, Sáez JC. Metabolic inhibition increases activity of connexin-32 hemichannels permeable to Ca2+ in transfected HeLa cells. Am J Physiol Cell Physiol. 2009; 297:C665–C678. [PubMed: 19587218]
16. Beblo DA, Wang HZ, Beyer EC, Westphale EM, Veenstra RD. Unique conductance, gating, and selective permeability properties of gap junction channels formed by connexin40. Circ Res. 1995; 77:813–822. [PubMed: 7554128]

NIH-PA Author Manuscript

NIH-PA Author Manuscript

NIH-PA Author Manuscript

17. Verselis VK, Ginter CS, Bargiello TA. Opposite voltage gating polarities of two closely related connexins. Nature. 1994; 368:348–351. [PubMed: 8127371]

18. Levit NA, Mese G, Basaly MG, White TW. Pathological hemichannels associated with human Cx26 mutations causing Keratitis-Ichthyosis-Deafness syndrome. Biochim Biophys Acta. 2012; 1818:2014–2019. [PubMed: 21933663]

19. Verselis VK, Trelles MP, Rubinos C, Bargiello TA, Srinivas M. Loop gating of connexin hemichannels involves movement of pore-lining residues in the first extracellular loop domain. J Biol Chem. 2009; 284:4484–4493. [PubMed: 19074140]

20. Teorell T. Transport processes and electrical phenomena in ionic membranes. Prog Biophys. 1953; 3:305–369.

21. Lin X, Gemel J, Beyer EC, Veenstra RD. Dynamic model for ventricular junctional conductance during the ventricular action potential. Am J Physiol Heart Physiol. 2005; 288:H1113–H1123.

NIH-PA Author Manuscript

NIH-PA Author Manuscript

NIH-PA Author Manuscript

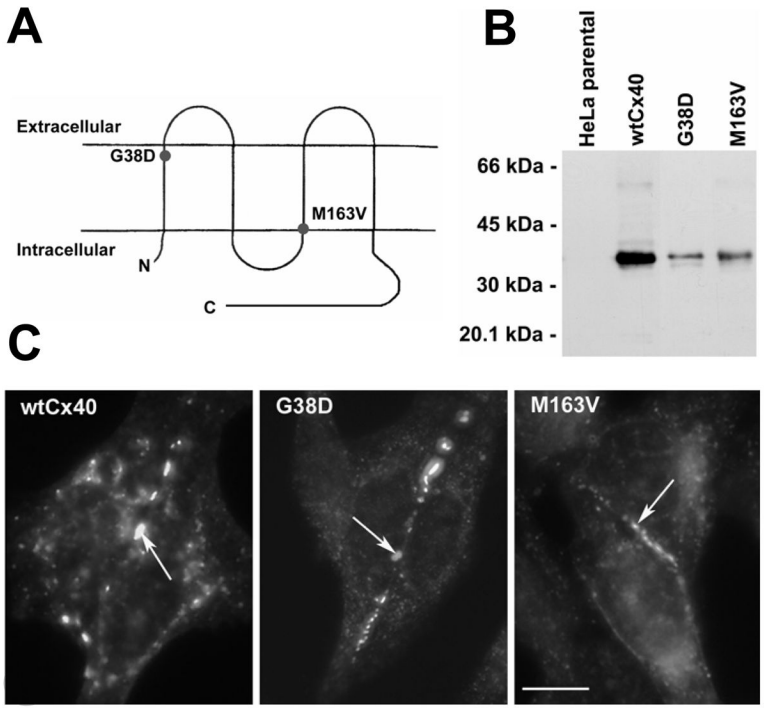

Figure 1.

G38D and M163V are produced and form gap junction plaques similarly to WTCx40 in HeLa cells. **A**, Membrane topology of Cx40 with the locations of G38D and M163V indicated by circles. **B**, Immunoblot detection of WTCx40, G38D, and M163V in homogenates of transiently transfected HeLa cells. **C**, Immunofluorescent detection of Cx40 in transiently transfected HeLa cells shows that WTCx40, G38D, and M163V localize to appositional membranes (arrows) as well as within the cytoplasm. Bar, 10 μm.

NIH-PA Author Manuscript

NIH-PA Author Manuscript

NIH-PA Author Manuscript

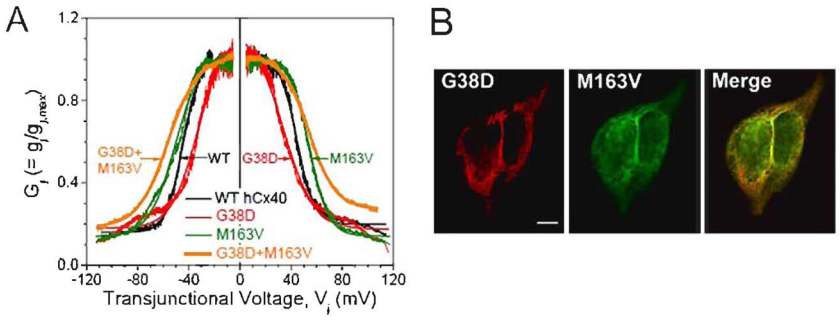

Figure 2.

Gap junctions formed by G38D, M163V, and the co-expressed mutants show altered V_j-dependent gating. **A**, Plots show the G_j-V_j relationships for homomeric WT (black), G38D (red), and M163V (green) gap junctions and co-expressed (heteromeric) G38D+M163V (orange) (The Boltzmann parameters for the fitted curves are listed in Table 1.). **B**, Confocal micrographs of double-label immunolocalization of G38D-mcherry (red) and M163V-GFP (green) in transiently co-transfected HeLa cells show extensive co-localization which appears yellow in the merged image. Bar, 8 μm.

NIH-PA Author Manuscript

NIH-PA Author Manuscript

NIH-PA Author Manuscript

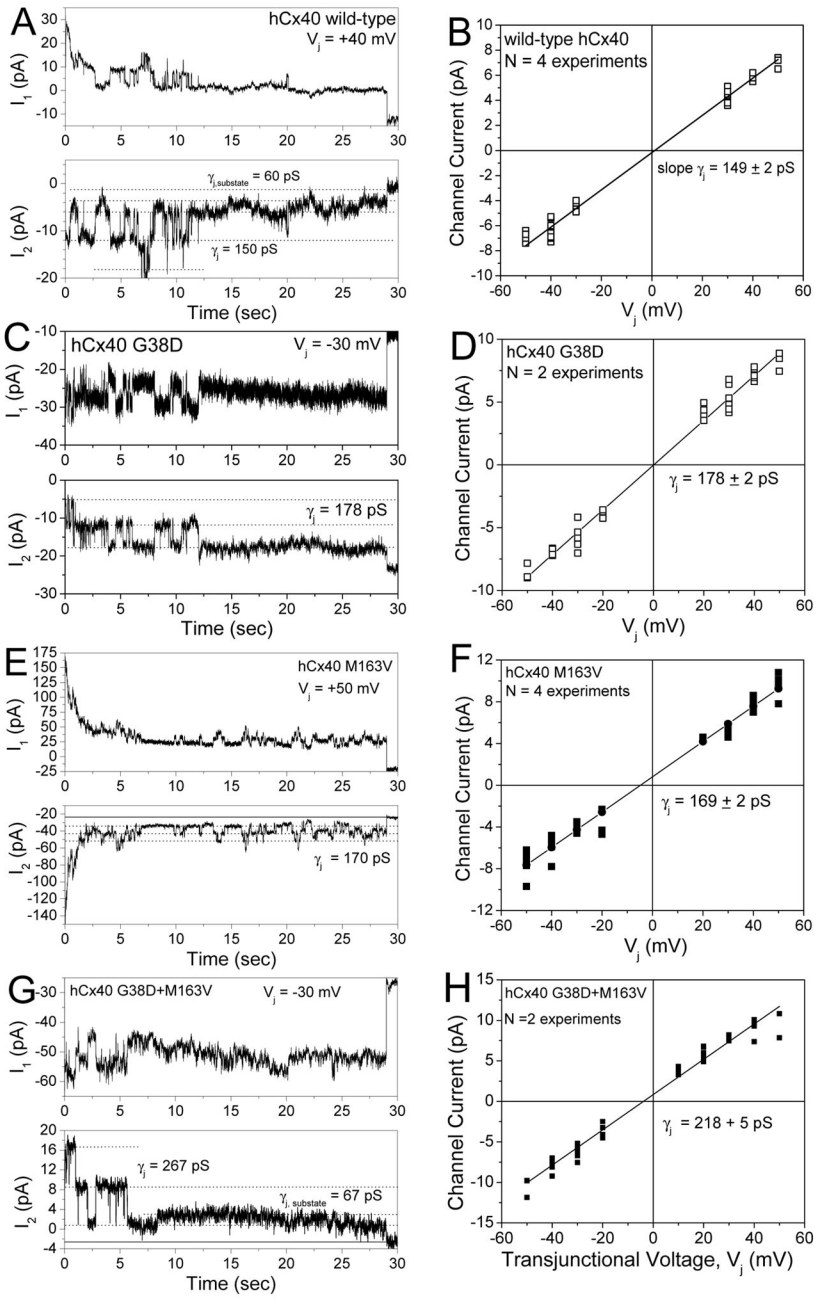

Figure 3.

Single channel conductances differ for WTCx40, G38D, and M163V gap junctions. **A**, Whole cell currents (I_1 and I_2) recorded simultaneously from WTCx40 N2a cell pair during a +40 mV V_j step applied to cell 1. Current amplitudes are indicated by dashed lines in the I_2 trace (I_j=-ΔI_2). **B**, I_j-V_j relationship for WTCx40 channels was generated from channel current amplitudes determined by Gaussian fits of the all points current histogram (not shown) for each 30 s V_j pulse. The mean slope conductance (γ_j) was 149±2 pS. **C**, Whole cell currents for a G38D channel during a −30 mV V_j pulse. **D**, I_j-V_j relationship for G38D. The mean slope γ_j was 178±2 pS. **E**, Whole cell currents for a M163V channel during a +50

NIH-PA Author Manuscript

NIH-PA Author Manuscript

NIH-PA Author Manuscript

mV V_j pulse. **F**, I_j-V_j relationship for M163V. The mean slope γ_j was 169±2 pS. **G**, Whole cell currents from a G38D+M163V expressing N2a cell pair illustrating a main channel conductance state of >220 pS and a <70 pS subconductance state. **H**, The mean channel current-voltage relationship for G38D+M163V gap junction illustrates its main open state slope γ_j of 218±5 pS.

NIH-PA Author Manuscript

NIH-PA Author Manuscript

NIH-PA Author Manuscript

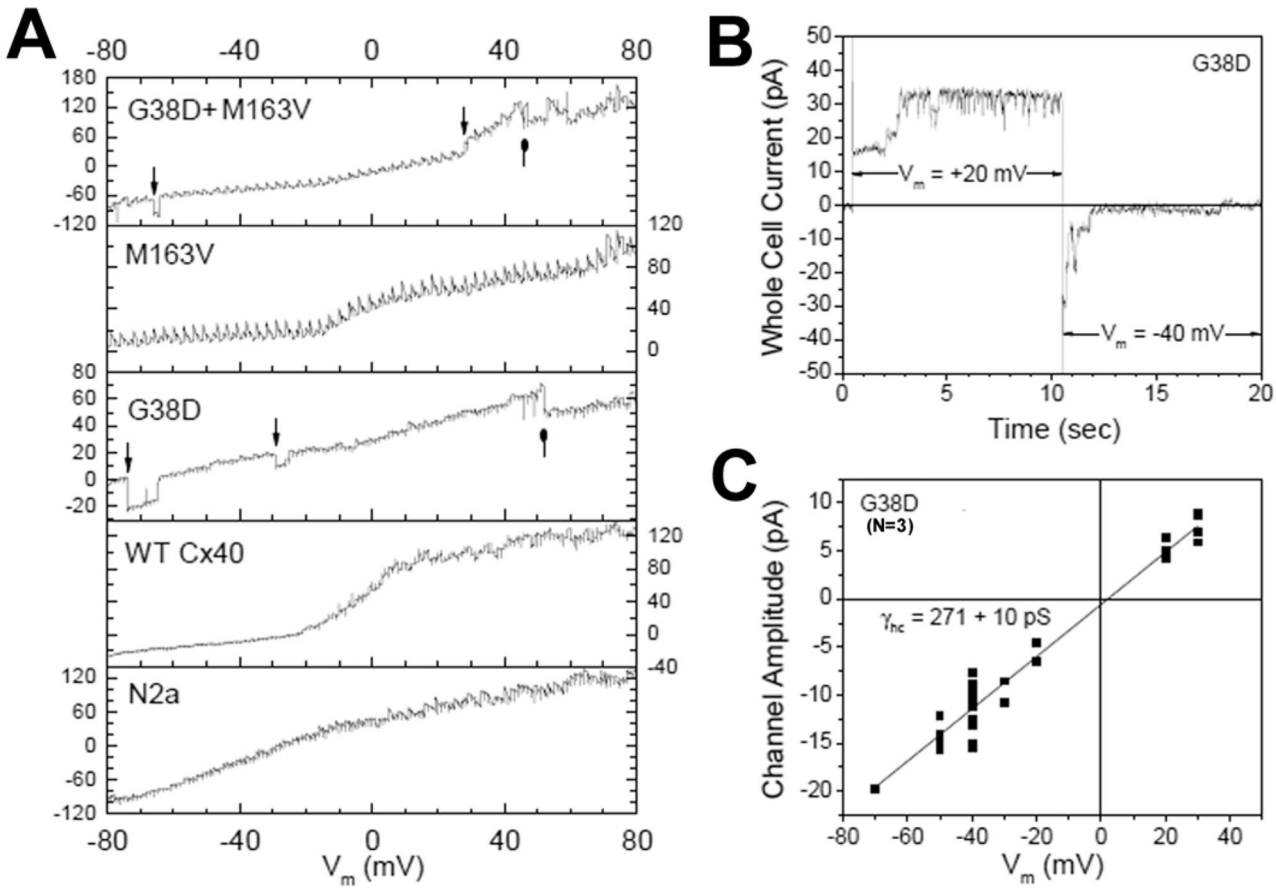

Figure 4.

Hemichannel activity of G38D mutant Cx40 channels. **A**, Single sweep whole cell current recordings from parental N2a, WTCx40, G38D, M163V, and G38D+M163V N2a cells in zero $CaCl_2$ saline during a V_m staircase protocol from −80 to +80 mV. High conductance channel openings and closings were evident only in cells expressing G38D. **B**, G38D hemichannel activity recorded during a +20 to −40 mV V_m step illustrates the activation and deactivation of this channel by depolarizing and hyperpolarizing V_m steps, respectively. **C**, Current-voltage relationship of the G38D hemichannel measured from three V_m step protocol experiments. The slope conductance, γ_{hc}, was 271±10 pS.

NIH-PA Author Manuscript NIH-PA Author Manuscript NIH-PA Author Manuscript

Table 1

V_j Gating Properties of Cx40 AF mutations

Connexin	−/+V_j	$G_{j,max}$	$G_{j,min}$	$V_{½}$ (mV)	Z (q)	Correlation Coefficient
WT Cx40	**−V_j**	1.001±0.002	0.160±0.001	−44.8±0.1	−3.91±0.03	0.96
(n=6)	**+V_j**	1.016±0.002	0.198±0.001	+44.6±0.1	+3.79±0.04	0.96
G38D	**−V_j**	1.109±0.008	0.179±0.002	−33.4±0.2	−2.47±0.04	0.93
(n=5)	**+V_j**	1.147±0.007	0.174±0.002	+34.0±0.2	+2.13±0.03	0.94
M163V	**−V_j**	1.04±0.003	0.139±0.002	−50.3±0.1	−2.44±0.03	0.95
(n=6)	**+V_j**	1.003±0.001	0.110±0.001	+54.4± 0.1	+3.37±0.02	0.97
G38D + M163V	**−V_j**	1.018±0.001	0.183±0.001	−56.2±0.1	−2.14±0.01	0.98
(n=5)	**+V_j**	1.017±0.001	0.273±0.001	+54.2±0.1	+2.43±0.01	0.99

Parameter values were derived from fitting the experimental G_j-V_j curves with a two state Boltzmann equation and are expressed as mean±SEM.

FEBS Lett. Author manuscript; available in PMC 2015 April 17.